NDT&E International 68 (2014) 105–112

Contents lists available at ScienceDirect

NDT&E International

journal homepage: www.elsevier.com/locate/ndteint

Accurate depth measurement of small surface-breaking cracks using an ultrasonic array post-processing technique

Maria V. Felice [a,b,*], Alexander Velichko [a], Paul D. Wilcox [a]

[a] Department of Mechanical Engineering, University Walk, University of Bristol, Bristol BS8 1TR, UK
[b] NDE Laboratory, Rolls-Royce plc., Bristol BS34 7QE, UK

ARTICLE INFO

Article history:
Received 1 April 2014
Received in revised form
6 August 2014
Accepted 8 August 2014
Available online 23 August 2014

Keywords:
Total focusing method
Full matrix capture
Crack sizing
Ultrasonic modelling

ABSTRACT

In this paper, the half-skip configuration of the Total Focusing Method (TFM) is used to image and size surface-breaking cracks. The TFM is an ultrasonic array post-processing technique which is used to synthetically focus at every image point in a target region. This paper considers the case of inspecting for cracks which have initiated from the far surface of a parallel-sided sample using an array on the near surface. Typically, only direct ray paths between the array and image points are included in the TFM algorithm and therefore the image obtained for this case consists only of root and tip indications; no specular reflection from the crack faces is captured. The tip indication often has such a poor signal-to-noise ratio that reliable crack depth measurement is challenging. With the Half-Skip TFM, instead of using directly-scattered signals, the image is formed using ultrasonic ray paths corresponding to the ultrasound that has reflected off the back surface and has then undergone specular reflection from the crack face back to the array. The technique is applied to experimental and simulated array data and is shown to measure the depth of small cracks (depth < 1 mm) with greater reliability than methods which rely on tip diffraction.

1. Introduction

1.1. Importance of crack sizing

The ability to reliably measure the depth of small surface-breaking cracks is very desirable in a range of high value industries including aerospace, petrochemical, power generation and nuclear. Knowledge of the presence of a crack whose depth is unknown normally results in automatic rejection of parts, both at manufacture and in service. This is an expensive practice and can cause significant disruption. If the depth of a crack is known, this information can be used in fracture mechanics calculations to allow a better estimate of the risk which the crack poses to the system [1]. It is particularly useful to be able to size small cracks accurately since these are the ones that will pose the least risk and are therefore most likely to be allowed.

1.2. Existing crack sizing methods

1.2.1. Overview of ultrasonic methods

There is a range of methods for defect sizing using single element ultrasonic probes (see [2,3] for a comprehensive review). These methods can be broadly divided into three:

1. Methods where the scattered signal from a defect is recorded and its amplitude compared to that of signals measured from artificial defects of different, known sizes [3].
2. Methods where a defect is scanned and the signal amplitude is measured at different probe position increments. An example is the 6 dB drop method [3] where the specular signal from a defect is maximized using a single probe and this probe is moved to the point where the signal drops by 6 dB. This point is taken to correspond to the edge of the defect and the process can be repeated for different scan directions to estimate the size of the defect.
3. Methods which rely on measuring the time-of-flight of different signals and deducing the defect dimensions from these. Bulk waves or surface waves can be used. An example is time-of-flight diffraction (TOFD) [4,5] where an ultrasonic probe is placed on either side of the location being inspected. If an embedded crack is present its size is determined using the time-of-flight of the ultrasonic signals scattered from its two tips. The technique can also be used to measure the depth of surface-breaking cracks as discussed in Section 1.2.2.

1.2.2. Time-of-flight diffraction (TOFD)

When using TOFD to measure the depth of a surface-breaking crack which is on the near side of the sample, the time-of-flight of the tip-diffracted signal is used to determine the crack depth. When the crack is on the far side, the location of the tip of the crack is determined and its location subtracted from the total

* Corresponding author at. Department of Mechanical Engineering, University Walk, University of Bristol, Bristol BS8 1TR, U.K. Tel.: +44 7935980127.
E-mail address: maria.felice@bristol.ac.uk (M.V. Felice).

http://dx.doi.org/10.1016/j.ndteint.2014.08.004

thickness of the sample to obtain a crack depth measurement. For cracks whose tip is close to the inspection surface, there might be significant overlap of the tip-diffracted signal and the lateral wave which travels between the transducers along the surface, as observed by Baby et al. [6]. The accuracy of the crack measurement depends on the ability to determine the arrival times accurately, which in turn depends on the resolution of the timing measurement system. The TOFD technique is dependent on the tip-diffracted signal which is weak.

Baby et al. [6] reviewed the use of TOFD for measuring the depth of surface-breaking cracks. They performed tests using longitudinal 45° angle beam 5 MHz probes on steel test blocks which contained vertical slits of depths varying from 0.91 mm to 30 mm. It should be noted that the slits used in this study were machined and had a width of 0.5 mm. The smallest slit whose depth they could determine was 1.82 mm deep. The depth results they obtained for the different slits had a mean error of ± 0.13 mm. They also found the technique to be successful at measuring the depth of slits inclined at angles of 10° and 15° to the surface and whose depths ranged from 2.56 mm to 19.82 mm.

1.2.3. Ultrasonic array methods

Ultrasonic arrays can be used to detect and size defects. Embedded defects from which specular reflections are captured can be sized using the 6 dB drop rule on the defect indications in array B-scans. This is similar to the 6 dB drop method described above but now the probe does not need to be moved. Surface-breaking cracks can be sized by measuring the distance between the tip and root indications in an array B-scan. In this case, typically a wedge is used to generate 45° shear waves in the sample.

More advanced methods can be used if the Full Matrix Capture (FMC) of data from the array is obtained. This is the set of A-scans for every transmit-and-receive element pair combination. The FMC data set is therefore the complete data set of an array [7] and any post-processing technique can be performed on it, including the Total Focussing Method (TFM) as well as more traditional scanning techniques such as plane B-scans, focused B-scans and sector scans. This flexibility is an advantage of opting for FMC and post-processing when using ultrasonic arrays, as opposed to the more traditional approach of beam forming.

The Total Focusing Method (TFM) is an ultrasonic array post-processing technique which is used to synthetically focus at every image point in a target region [7] and which requires the FMC of data from the array. One possible method of sizing defects which are larger than two wavelengths is to obtain a TFM image from a single location and then use the 6 dB drop rule on the defect indication by comparing intensity of pixels [8]. An FMC-based method has also been developed to size smaller defects, including sub-wavelength defects, and this utilizes scattering coefficient matrices which describe the ultrasonic wave scattered from a defect for different incident and scattered angles [8,9]. Both these FMC-based methods are only applicable to defects which are embedded (not surface-breaking or close to any surface) and from which specular reflections are obtained, such as delamination in composites.

1.3. TFM for surface-breaking cracks

This paper presents a new approach for imaging and sizing small surface-breaking cracks using the Half-Skip TFM [10] which is a modification to the TFM. Therefore it is important to first describe the application and limitations of the TFM when used for imaging and sizing small surface-breaking cracks.

Consider the inspection of a sample with two flat parallel surfaces and of thickness h (Fig. 1a). A surface-breaking crack grows out of the lower surface and an array is placed on the opposite surface. The crack grows at an angle θ_{tilt} relative to the surface normal. The crack depth, d, is the vertical distance between the sample's lower surface and the tip of the crack. This is equal to the distance along the crack face when $\theta_{tilt}=0°$. The line joining the centre of the array to the point where the crack initiates makes an angle of θ_{test} with the vertical. The horizontal distance between the centre of the array and the point where the crack initiates from is equal to $h \tan \theta_{test}$.

In the conventional TFM only direct ray paths between the array and image points are included. For the case in Fig. 1a, an indication from the length of the back surface directly below the array is obtained together with an indication from the crack. In the case of a surface-breaking crack that is detected at an oblique incident angle (for example $\theta_{test}=45°$), the resulting indication consists only of root (corner) and tip indications. The crack depth, d, can be determined by measuring the vertical distance between these two indications. This is presented in Fig. 4a and b in Section 3.2. For cracks that have a small depth, the tip indication can be indistinguishable from the root indication. For cracks that are very narrow, this tip indication can have a very poor signal-to-noise ratio and this is exacerbated in materials which have a high degree of microstructural scattering. Therefore, small or narrow cracks in scattering materials often cannot be sized using this technique.

When a crack is detected at normal incidence ($\theta_{test}=0°$), a tip indication is visible in the TFM image together with a decrease in amplitude in the centre of the back surface indication (Fig. 1b). The crack depth, d, can be determined by measuring the vertical distance between the tip indication and the back surface, but again this is made difficult or impossible when the material is noisy, when cracks are short or narrow, or a combination of these factors.

Consider the inspection of a surface-breaking crack with $\theta_{test}=45°$. Simple ray tracing will indicate that the majority of ultrasonic energy that is scattered by the crack and received by the array has reflected off the back surface. The ray paths that have interacted directly with the crack i.e. without reflections off the back surface, have done so by tip diffraction and these signals are weak. Therefore, in post-processing it seems preferable to

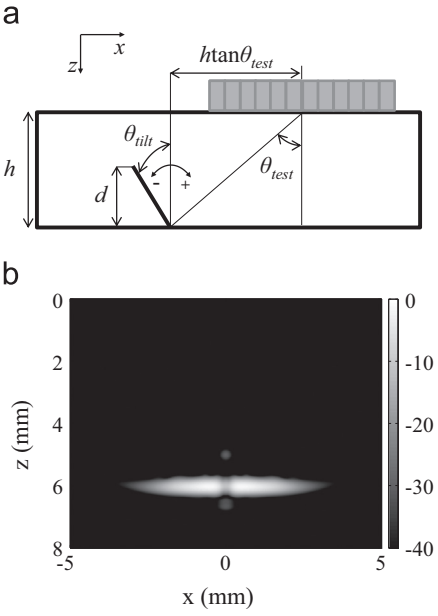

Fig. 1. (a) Schematic showing relative position of array and crack. (b) TFM image obtained using simulated array data for the configuration in (a) when $h=6$ mm, $d=1$ mm, $\theta_{tilt}=0°$ and $\theta_{test}=0°$. Note that the amplitude is on a dB scale, normalized to the maximum value in the image.

consider the ray paths that have reflected off the back surface instead of the direct ray paths. This is exactly what is done in the Half-Skip Total Focusing Method [10], referred to in this paper as the HSTFM.

The aim of this paper is to outline some of the advantages and limitations of using the HSTFM for imaging and sizing surface-breaking cracks. A computer model was used to simulate array data on which the algorithm could be tested extensively; this is described in Section 2. In Section 3, the HSTFM algorithm is described in detail and is applied to simulated array data. In Section 4, the HSTFM algorithm is applied to experimental data which was collected from electric discharge machined (EDM) notches as well as real cracks.

2. Simulation of ultrasonic array data

Simulation tools have a major role to play when developing a novel NDE technique because they allow the influence of various parameters on the performance of the technique to be studied [11]. In this section, the model used to simulate time-domain array data is described. In particular, it is the Full Matrix Capture of data which is simulated and this data is used to study the influence of parameters, such as inspection frequency, on the performance of the HSTFM.

A hybrid modelling approach is taken which consists of two parts; the generation of the scattering coefficient matrix for a particular crack and ray tracing to simulate the ultrasonic paths between a particular array and the crack. The entire model is implemented in MATLAB (MathWorks Inc., Massachusetts, USA).

2.1. Use of scattering coefficient matrices

The scattering coefficient matrix, or S-Matrix, of a crack describes the amplitude of the scattered wave that would be measured if the distance from crack to receiver was normalized to one wavelength [12]. For the 2D case, it can be represented by a 2D plot of scattered amplitude at a particular frequency plotted against incident angle, θ_{in}, and scattered angle, θ_{sc}.

The use of S-Matrices is particularly useful when simulating array data for two reasons. Firstly, the S-Matrix of a crack depends only on frequency and not on any other inspection factors such as element pitch or number of elements. Therefore, S-Matrices at different frequencies need to only be obtained once per crack and then can be used to simulate the ultrasonic response for different arrays, for example when optimizing an array design. Secondly, understanding how cracks scatter ultrasound as a function of incident and scattered angles is in line with the concept of arrays, where the different elements each correspond to different inspection angles relative to a crack location.

2.2. Finite Element method

A Finite Element method is used to generate the S-Matrices in this paper because analytical solutions for the ultrasonic scattering from surface-breaking cracks do not exist. Usually Finite Element (FE) methods have the disadvantage of being extremely time-consuming but in this paper an efficient FE method is used [13]. This method can be used for surface-breaking cracks [14] and for cracks of arbitrary shapes, such as stress corrosion cracks [15].

Previously, the Finite Element Local Scattering (FELS) method was developed which was more efficient than conventional FE methods because only the scatterer (e.g. a crack) and the immediate space around it were modelled, instead of the scatterer inside an entire part [16]. However, an absorbing region was required to absorb the scattered field and prevent it being reflected back onto the scatterer, and this region could contain up to 90% of all nodes in the model. The improved method [13] goes one step further by eliminating the need for this absorbing region by implementing non-reflecting boundary conditions. In addition, the loading nodes (where the incident ultrasound is excited) and the monitoring nodes (where the scattered ultrasound is measured) are now located on the surface of the scatterer. Therefore, the modelling domain consists of just one layer of elements around the scatterer and this greatly reduces the computing power and time required.

2.3. Hybrid model

Once the S-Matrices of a crack are obtained for different frequencies, they are stored and then used in conjunction with ray tracing to generate the FMC data for a particular array at a particular location with respect to the crack. The FE method is performed in the frequency, ω, domain whilst the array input signal, $u(t)$, is in the time, t, domain. Therefore, the frequency spectrum, $U(\omega)$, of the input signal must be calculated and this is done using the Fourier Transform, F, defined as

$$U(\omega)=\mathcal{F}(u(t))=\int_{-\infty}^{\infty}u(t)\exp(-i\omega t)dt \tag{1}$$

Once the frequency spectrum of the input signal is obtained, the S-Matrices of the sample frequencies are retrieved. The calculations described below are then performed in the frequency-domain for each sample frequency. After this, the Inverse Fast Fourier Transform is used to generate the time-domain FMC data.

Consider an array with an element, T, operating in transmission and an element, R, operating in reception in a 2D space. A scatterer is located so that the array is in its far field, which means it is at a sufficient distance from the scatterer that the scattered field exhibits no further radial dependence other than decay due to beam spread. This scenario is represented in Fig. 2 for the case of a surface-breaking crack. Distances, $r_{T,R,B}$ and angles, $\theta_{T,R,B}$ are calculated using trigonometry (Fig. 2).

In the frequency domain, for an input signal of $U(\omega)$, the received signal $U_{TR}^{C}(\omega)$ due to the presence of the crack is given by:

$$U_{TR}{}^{C}(\omega)=\exp(ik(r_T+r_R))\left(\frac{2\pi}{kr_Tr_R}\right)^{0.5}D(\omega,\theta_T)D(\omega,\theta_R)S(\theta_T,\theta_R,\omega)U(\omega) \tag{2}$$

where $k=\omega/c$, c is the ultrasonic velocity, r_T is the distance between the centre of the scatterer and the transmitting element, r_R is the distance between the centre of the scatterer and the receiving element, θ_T is the angle a line between the scatterer and the transmitting element makes with the vertical, θ_R is the angle a line between the scatterer and the receiving element makes with the vertical, D is element directivity and S is the S-Matrix. Note that in the case of surface-breaking cracks, the centre of the scatterer in the FE simulations, and consequently also in the ray tracing, is taken as the centre of the crack on the back surface. The first term in Eq. (2) accounts for the shift due to the ultrasound propagation path, the second term accounts for beam spread and the third and fourth terms account for element directivity $D(\omega,\theta)$ which for the longitudinal mode is given by [17]:

$$D(\omega,\theta)=\left(\frac{\sin((1/2)ka\ \sin\theta)}{(1/2)(ka\ \sin\theta)}\right)\left(\frac{(\alpha^2-2\ \sin^2\theta)\cos\theta}{F_0(\sin\theta)}\right) \tag{3}$$

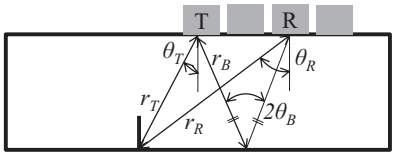

Fig. 2. Schematic showing the angles and distances used in the hybrid model.

where a is the array element width, α is the ratio of longitudinal to transverse wave velocities, which is a function of the Poisson's ratio and

$$F_0(\zeta) = (2\zeta^2 - \alpha^2)^2 - 4\zeta^2(\zeta^2-1)^{0.5}(\zeta^2-\alpha^2)^{0.5} \quad (4)$$

It can easily be shown numerically that the second term in Eq. (3) can be approximated by cos θ when the Poisson's ratio is in the region of 0.3 which is the case for most typical engineering materials, including those considered in this paper. Therefore, this approximation was used in this paper.

The S-Matrix of a scatterer by definition describes the additional wavefield due to the scatterer. Therefore, the S-Matrix contains information about both the back-scattered (i.e. reflected) field and the forward scattered field that by interference with the original field leads to shadowing. To simulate the correct FMC data of a surface-breaking crack it is necessary to sum the FMC data obtained using the S-Matrix to the FMC data obtained in the absence of a crack from a complete back surface. The latter is obtained by computing the ultrasound that has undergone specular reflection from the back surface for each transmit-and-receive element pair combination.

In the frequency domain, the ultrasound received by the array from the back surface in the absence of a crack, $U_{TR}^{B}(\omega)$, is given by:

$$U_{TR}{}^{B}(\omega) = \exp(ik(2r_B))\left(\frac{1}{2r_B}\right)^{0.5} D(\omega,\theta_B)^2 R_C(\theta_B) U(\omega) \quad (5)$$

where r_B is the distance between the transmitting or receiving element and the midpoint between them projected onto the back surface, θ_B is the angle between the vertical and the line joining the transmitting or receiving element to this point as shown in Fig. 2, and $R_C(\theta)$ is the reflection coefficient which, for incident and reflected waves that are both in the longitudinal, l, mode, is given by:

$$R_C(\theta_l) = \frac{(c_{tr}/c_l)^2 \sin 2\theta_l \sin 2\theta_{tr} - \cos^2 2\theta_{tr}}{(c_{tr}/c_l)^2 \sin 2\theta_l \sin 2\theta_{tr} + \cos^2 2\theta_{tr}} \quad (6)$$

where subscript tr refers to the transverse mode and hence by Snell's law:

$$\sin\theta_{tr} = (c_{tr}/c_l)\sin\theta_l \quad (7)$$

In the frequency domain, the overall signal received, $U_{TR}(\omega)$, is given by the summation:

$$U_{TR}(\omega) = U_{TR}{}^{C}(\omega) + U_{TR}{}^{B}(\omega) \quad (8)$$

The equivalent time-domain signal, $u_{TR}(t)$, is obtained using the Inverse Fourier Transform:

$$u_{TR}(t) = \mathcal{F}^{-1}\{U_{TR}(\omega)\} \quad (9)$$

3. Half-Skip Total Focusing Method (HSTFM) algorithm

3.1. Conventional and Half-Skip TFM algorithms

In the Total Focusing Method (TFM) the beam is synthetically focused at every point in the target region [7] as follows. After obtaining the FMC data, the target region, which is in the x–z plane in 2D (Fig. 1), is discretized into a grid. The signals from all elements in the array are then summed to synthesize a focus at every point in this grid. Linear interpolation of the time domain signals is necessary since they are discretely sampled. The intensity of the TFM image I_{TFM} at any point (x,z) is given by:

$$I_{TFM}(x,z) = \left|\sum H_{TR}\left(\frac{1}{c}\left(\sqrt{(x_T-x)^2+z^2}+\sqrt{(x_R-x)^2+z^2}\right)\right)\right| \quad \text{for all } T,R \quad (10)$$

where $H_{TR}(t)$ is the Hilbert transform of a signal $u_{TR}(t)$ in the FMC data, x_T is the x-position of the transmitting element (T) and x_R is the x-position of the receiving element (R). Note that the z-position of all elements is zero (Fig. 3a). The summation is carried out for all possible transmitter–receiver pairs and therefore uses all the information captured with FMC. This algorithm is referred to as 'conventional TFM' in this paper.

As shown in Eq. (10), in order to generate a TFM image, the time taken to travel between each array element and each point, $P(x,z)$, in the imaging space must be computed. In conventional TFM, the time taken to travel between an element and a point, P, is the same in transmission and reception (Fig. 3a). In the HSTFM this is not the case because now the ultrasound of interest is that which has been reflected off the back surface before undergoing specular reflection from the crack surface back to the array [10]. Therefore, the time taken to travel between an array element and a point P is longer in transmission than in reception because of this reflection off the back surface (Fig. 3b).

A point, $P_m(x_m, z_m)$, is defined (Fig. 3c) such that the single line between it and the transmitting element is equivalent to the ray path between the transmitting element and $P(x,z)$ via a reflection from the back surface. For a straight crack normal to a smooth back surface which is at location $z=h$, P_m is in the mirrored location of P about the back surface. Therefore, $x_m=x$ and z_m is given exactly by:

$$z_m = 2h - z \quad (11)$$

The equation for the HSTFM algorithm can then be given by:

$$I_{HSTFM}(x,z) = \left|\sum H_{T,R}\left(\frac{1}{c}\left(\sqrt{(x_T-x)^2+z^2+4h(h-z)}+\sqrt{(x_R-x)^2+z^2}\right)\right)\right| \quad \text{for all } T,R \quad (12)$$

3.2. Application of the HSTFM algorithm to simulated array data

Full Matrix Capture (FMC) data was simulated for a 20 MHz ultrasonic array (Array 1 in Table 1) and a surface-breaking crack of $\theta_{tilt}=0^\circ$ and $d=1$ mm in a sample of $h=6$ mm (Fig. 1a). The material properties used in the simulation were of titanium with an ultrasonic longitudinal wave velocity of 6000 m/s. The array was positioned such that $\theta_{test}=45^\circ$. The centre of the array was at $x=0$ mm. The HSTFM algorithm was applied to the FMC data and the resulting image is shown in Fig. 4c. The conventional TFM image obtained from the same FMC data is shown in Fig. 4a.

The depth of the crack is measured from the HSTFM image using the 6 dB drop rule as follows. The x-position of the centre of the

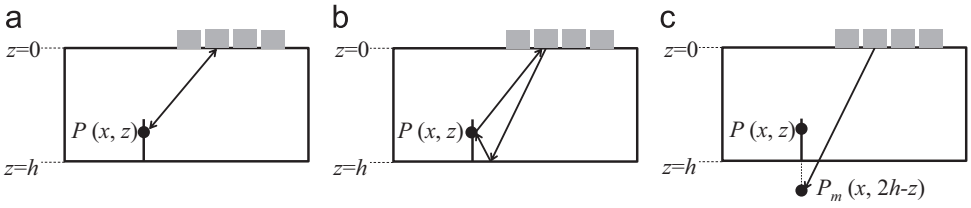

Fig. 3. (a) Example of the direct ray path which is considered in the conventional TFM, (b) example of the ray path which is considered in the HSTFM, and (c) position of point, P_m, used in the HSTFM calculation.

crack root, x_c, is determined from the crack indication in the conventional TFM image. The value of x_c is taken to be equal to the x-position of the pixel of maximum amplitude in this indication. The amplitude of the HSTFM image for the value of $x=x_c$ is plotted against vertical distance, z. The peak amplitude is determined and the '−6 dB amplitude' is calculated. The z values of the two points on the plot which have an amplitude equal to the '−6 dB amplitude' are located. The crack depth is assumed equal to half the difference between these two points since the crack indication is double the true crack indication and symmetrical about the depth of the back surface, as explained below. Fig. 4d is a plot of amplitude versus vertical distance at $x=x_c=-6$ mm in Fig. 4c, and the depth of the crack is calculated to be 0.98 mm. For the conventional TFM image of the same crack, the depth of the crack is determined by measuring the distance between the peak of the root indication and the peak of the tip indication (Fig. 4b) and is found to be 1.05 mm.

In the HSTFM image, half of the crack indication is above the location of the back surface and half is beneath it. This is because the equivalent point, P_m, is calculated for points both above and below the back surface and this has the effect of doubling the crack indication. Physically, for points above the back surface, the ultrasonic paths being considered are reflections off the back surface to point P and direct paths from this point back to the array element. Physically, for image points, P, below the back surface, the point, P_m, is above the back surface. The ultrasonic paths being considered in this case are direct paths to the point P_m (not P because no ultrasonic paths reach P in reality) and then reflections off the back surface back to the array element. The shape is symmetrical about the back surface because the exchange of P and P_m does not alter the ray path length.

Table 1
Array parameters. Note that all imaging is based on the longitudinal mode.

Array parameter	Array 1	Array 2	Array 3
Centre frequency (MHz)	20	10	5
Number of elements	32	32	32
Element pitch (mm)	0.150	0.150	0.150
Element pitch (wavelengths)	0.500	0.250	0.125

The apparent 'smearing' of the back surface indication can be explained [10]. It is due to the finite duration signals reflected from the back surface being 'smeared out' due to the closeness in time of arrival of the back surface reflection and these image points when using HSTFM. This artefact is symmetrical about the back surface for the same reason as the crack indication is.

Array data was simulated for 5 MHz, 10 MHz and 20 MHz arrays (full details in Table 1) for a range of crack depths, d, and $\theta_{tilt}=0^\circ$ and a sample of $h=6$ mm. In all cases, the width of the crack was 0.025 mm. For the 10 MHz and 20 MHz arrays, values of d between 1/3 wavelength and 8 wavelengths were considered. For the 5 MHz array, values of d between 1/3 wavelength and only 4 wavelengths were considered since for this frequency, the thickness of the part was equal to 5 wavelengths. The location of the crack with respect to the array was such that $\theta_{test}=45^\circ$ (Fig. 1a). The results are shown in Fig. 5 together with experimental data points (Section 4). They are plotted as measured crack depth versus nominal crack depth, in number of wavelengths, λ. The resulting lines do not overlay the 1:1 line but are monotonically increasing and linear over a long range.

For values of d which are less than 1.8 wavelengths, the relationship between measured and nominal depths is not monotonic. This is expected because the crack size is close to the diffraction limit. The Point Spread Function (PSF) is defined as the response of an imaging system to the ideal point scatterer [18]. The PSF was simulated for the 20 MHz array and the HSTFM algorithm for a point scatterer at $x=-6$ mm, $z=6$ mm. Using the −6 dB rule, the indication had a vertical height of 1 mm, or a half vertical height of 0.5 mm (1.7λ). As expected, this is close to the crack depth above which a monotonic increase is observed.

For 10 MHz, for values of d which are greater than approximately 6 wavelengths, and for 5 MHz, for values of d which are greater than approximately 3 wavelengths, the relationship is no longer linear. This is probably because in these regions $d>3$ mm i.e. $>50\%$ of the sample thickness. Therefore, specular reflection from the upper portion of the crack (towards its tip) is only possible at very shallow angles, relative to the inspection surface.

Array data was simulated for the 20 MHz array, a crack of $d=1$ mm, $\theta_{tilt}=0^\circ$ and the horizontal distance between the centre of the array and the crack ranging from 3 mm to 12 mm such that θ_{test} varied from 27° to 63°. Smaller values of θ_{test} were not considered because the active length of the array is 4.8 mm and

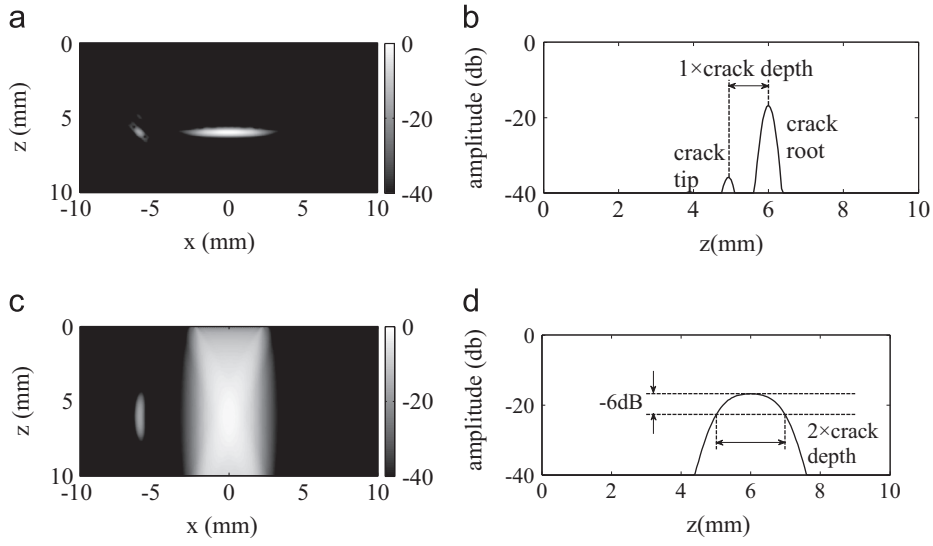

Fig. 4. (a) Conventional TFM image of a 1 mm deep crack with $\theta_{test}=45^\circ$. (b) Measurement of crack depth using plot of amplitude at $x=x_c=-6$ mm in (a) versus vertical distance, z. (c) HSTFM image of a 1 mm deep crack with $\theta_{test}=45^\circ$. (d) Measurement of crack depth using plot of amplitude at $x=x_c=-6$ mm in (c) versus vertical distance, z. Note that the amplitude is on a dB scale, normalized to the maximum value in the 2D image.

its indication (values above −30 dB; 0 dB being the maximum amplitude of the back surface indication) is approximately 5.4 mm in length. Therefore, if the horizontal distance between the centre of the array and the crack was smaller than 5.4/2 mm the crack indication would coincide with the back surface indication. The results of this study are presented in Fig. 6a and show that for values of θ_{test} up to 60° the measured crack depth is within ±0.1 mm (10%) of the nominal crack depth. This means that the HSTFM can be used for a range of inspection angles and is not limited to 45° inspections. Using an array with a shorter active length might enable smaller values of θ_{test} to be used.

Array data was simulated for the 20 MHz array, $\theta_{test}=45°$ and a tilted crack of $d=1$ mm with θ_{tilt} ranging from −10° to 10°. The results of this study are presented in Fig. 6b and show that for values of θ_{tilt} between −6° and 4° the measured crack depth is within ±0.1 mm (10%) of the nominal crack depth. The higher value in the negative direction (Fig. 1a) might be due to the fact that more of the specularly reflected signals from the crack surface are reflected back to the array, as opposed to the back surface, when the crack is tilted away from the array.

4. Experimental validation of the HSTFM algorithm

4.1. Sizing of EDM notches

For the experimental validation, an array with a centre frequency of 18 MHz, manufactured by IMASONIC SAS (Haute-Saône, France) was used. It had the same number of elements and element pitch as the arrays used in the simulations (Table 1). A stepped titanium test piece was used which had three electric discharge machined (EDM) notches: 0.5 mm deep and 1 mm deep in 6 mm thickness of the material and 2 mm deep in 4 mm thickness of the material. Full Matrix Capture data was collected from the three notches, with the array positioned so that $\theta_{test} \approx 45°$ (Fig. 1a). The notches had a width of approximately 0.25 mm. The FMC data was processed using both the conventional TFM and the HSTFM. The experiments were repeated for a 10 MHz array with the same properties as Array 2 in Table 1. The results obtained from the HSTFM are shown in Fig. 5 together with the simulated results and show good agreement.

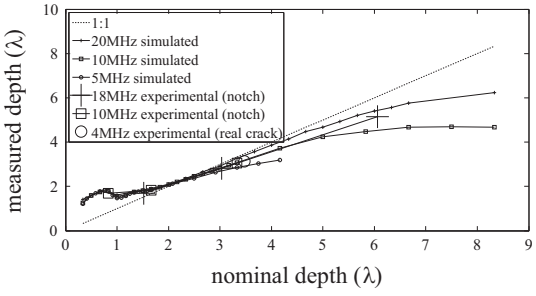

Fig. 5. Plot of measured depth (wavelengths) using the HSTFM versus nominal depth (wavelengths) for a range of crack depths and array frequencies, using both simulated and experimental data.

The experimental results obtained for the 18 MHz array and 0.5 mm notch (1.5λ) are of particular interest because they demonstrate how the HSTFM can be used to size small cracks which the conventional TFM cannot. As shown in Fig. 7 it is impossible to size this notch using the conventional TFM image shown since the location of the tip cannot be determined. However, its depth is measured to be 0.56 mm from the HSTFM image.

The depth of this notch is just outside the monotonic portion of the graph in Fig. 5 and the measured depth value corresponds to more than one nominal depth value. Therefore, if a HSTFM measurement of 0.56 mm were to be obtained from a crack of unknown depth, it is possible that this measurement would be incorrect. However, even if this is the case, the HSTFM measurement gives a maximum possible depth of the crack. With the TFM, when only the crack root indication is visible there is no guarantee that the crack is smaller than the width of the root indication; it might be that the crack is deeper than this but its tip is not visible.

4.2. Application of technique to real cracks

Experimental array data was also collected from two real cracks: one in a titanium sample of 3 mm thickness and one in an austenitic stainless steel sample of 40 mm thickness (ultrasonic longitudinal wave velocity=5760 m/s). This was done to demonstrate that HSTFM is applicable to real surface-breaking cracks as well as EDM notches and to demonstrate how HSTFM is advantageous over TFM in noisy material.

For the titanium sample, FMC data was obtained using the 18 MHz array and the conventional and Half-Skip TFM images were computed (Fig. 8a and b). Fig. 8c shows plots of amplitude versus depth through three values of x: position of the crack in Fig. 8a (A), position of no crack in Fig. 8a i.e. noise (B) and position of the crack in Fig. 8b (C). The points required to measure the crack depth for each technique are marked in Fig. 8c and it is clear that the HSTFM is advantageous compared to the conventional TFM for noisy materials.

For the thicker, steel sample, FMC data was obtained using a 4 MHz array (32 elements, 1 mm element pitch) and the conventional and Half-Skip TFM images were computed (Figs. 8d and e). The crack was produced in a controlled laboratory environment and has a nominal depth of 5 mm. It is not possible to measure the depth of the crack from the conventional TFM image since the tip is not visible whilst the depth was measured to be 4.5 mm from the HSTFM image. A data point referring to this crack was plotted on Fig. 5 and shows good agreement with the simulated results.

In order to confirm the sizing capability of the HSTFM for these real cracks it will be necessary to cut up the samples and measure the cracks directly. However, what has been confirmed is that the technique was successfully applied to two different materials of different thicknesses and improved crack indications were obtained compared to using the conventional TFM.

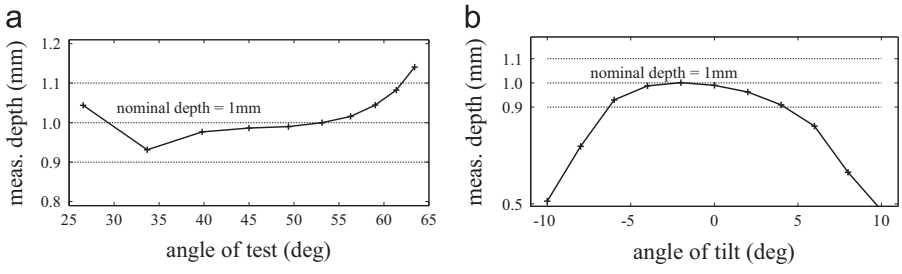

Fig. 6. (a) Plot of measured depth (mm) versus angle of test (deg). (b) Plot of measured depth (mm) versus angle of tilt of crack (deg). Note: in both (a) and (b) simulated 20 MHz array data is used.

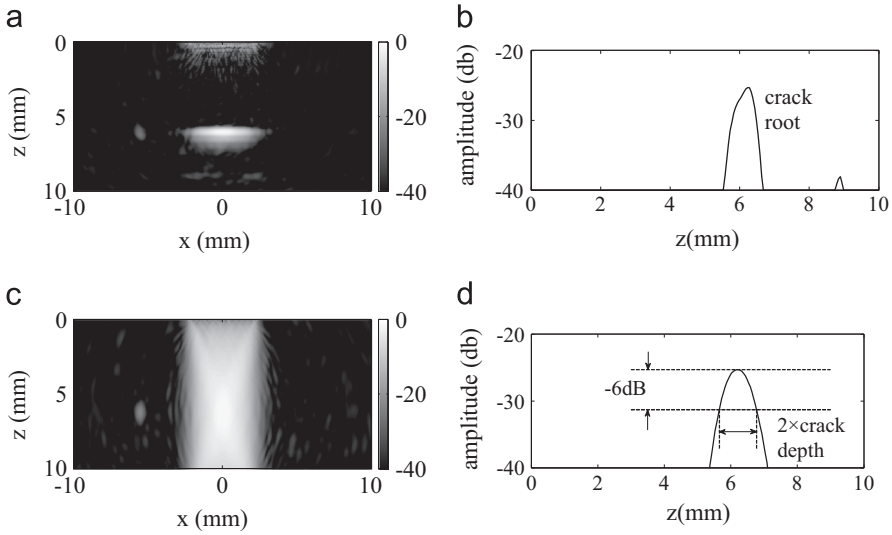

Fig. 7. (a) Conventional TFM image of a 0.5 mm deep notch. (b) Plot of amplitude at $x=x_c=-6$ mm in (a) versus vertical distance, z. (c) HSTFM image of the same 0.5 mm deep notch as in (a). (d) Plot of amplitude at $x=x_c=-6$ mm in (c) versus vertical distance, z. The array used has a centre frequency of 18 MHz. Note that the amplitude is on a dB scale and in both the TFM and HSTFM images is normalized to the maximum in the 2D TFM image.

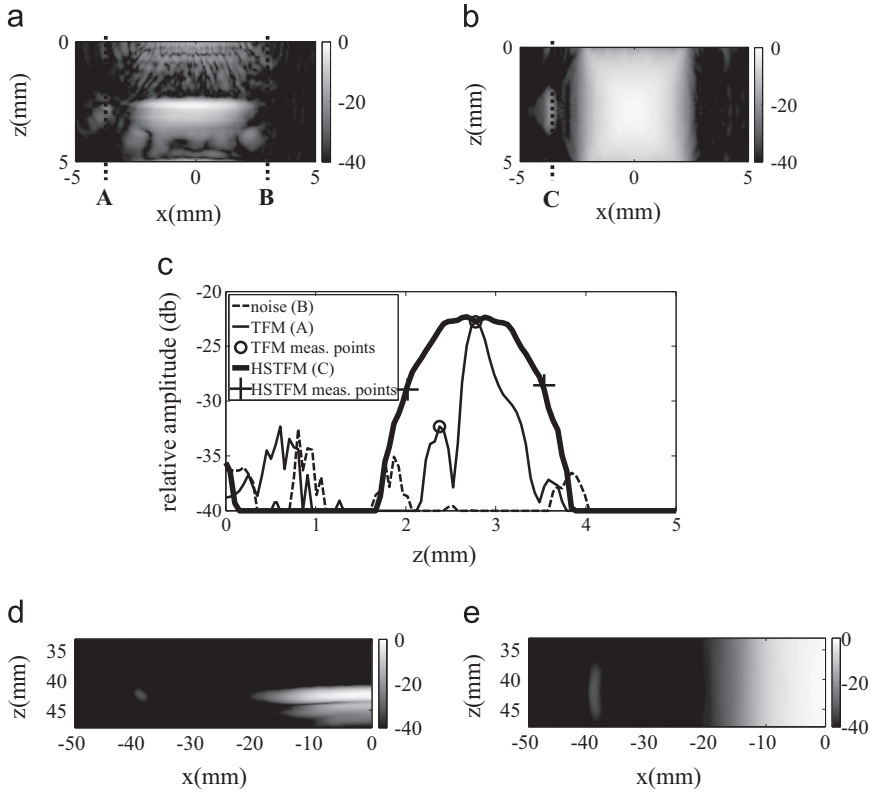

Fig. 8. (a) Conventional TFM image of a real crack in a titanium sample of thickness ≈ 3 mm. (b) HSTFM image of the same crack as (a). (c) Plot of amplitude versus vertical distance, z, for x-positions A, B and C in (a) and (b). (d) TFM image (detail) of a real crack in a steel sample of thickness ≈ 40 mm. (e) HSTFM image (detail) of the same crack as (d). Note that the amplitude is on a dB scale and for each crack, the amplitude in both the TFM and HSTFM images is normalized to the maximum in the corresponding TFM image.

5. Discussion

The Half-Skip TFM has been found to be more reliable for measuring the depth of small surface-breaking cracks than the conventional TFM because it does not rely on the signal diffracted from the crack tip. There are some particular cases where this advantage results in being able to size cracks with the HSTFM which cannot be sized with the conventional TFM. Firstly, when cracks have a small depth, the tip signal is not distinguishable from the crack root signal in the conventional TFM image so the crack cannot be sized (Fig. 7). When cracks are so small that the HSTFM measurement is also inaccurate (Fig. 5), the HSTFM measurement value is still useful because it is the maximum possible depth of the crack. With the TFM this is not the case because when only a crack root indication is visible there is no guarantee that the crack is smaller than the root indication.

Secondly, when cracks are present in noisy material, the tip signal can be of a similar level to the noise level (Fig. 8a–c). With the HSTFM it is not necessary to locate the crack tip, only to locate the crack root and the −6 dB points from it, which are typically well above the noise level.

A third case where the HSTFM should outperform the conventional TFM is for cracks with a very small width and this needs to be studied further. It is expected that because HSTFM does not rely on tip diffraction, its sizing capability will not be dependent on crack opening, so long as the crack faces are not in complete contact.

As well as increasing sizing accuracy, the HSTFM provides a clearer indication of small cracks than the conventional TFM does, since an indication is obtained from the entire extent of the crack face and not just the root and possibly the tip. As for the conventional TFM, the HSTFM only requires one probe in contrast to TOFD and the processing technique is performed in post-processing so data can be collected quickly and then processed and analysed offline.

This work is an initial study and more work is required to explore the effect of different crack parameters, e.g. crack tilt, and the interaction between parameters. The plot of measured depth versus nominal depth can potentially be used as a calibration curve in all portions where it is increasing monotonically. However, a better understanding of the relationship between measured and nominal crack depths for different sample thicknesses is required. This will include studying the sizing capability for varying ratios of crack depth to sample thickness. As the crack depth approaches the sample thickness, specular reflection from the upper portion of the crack is only obtained at very shallow angles, relative to the inspection surface.

6. Conclusion

This paper has investigated the capability of the Half-Skip TFM for sizing surface-breaking cracks. With the HSTFM, the specular reflection from the faces of surface-breaking cracks is captured. The technique has been successfully applied to simulated and experimental array data and has been shown to be better at measuring the depth of small cracks and the depth of cracks in noisy materials than the conventional TFM.

Acknowledgements

This work was supported by the Engineering and Physical Sciences Research Council through the Industrial Doctorate Centre in NDE (Grant no. GR/T18783/01). M V Felice is also supported financially by the Royal Commission for the Exhibition of 1851. The steel sample was kindly provided by the NDE team at Rolls-Royce Naval Marine, Derby, UK.

References

[1] Guide to methods for assessing the acceptability of flaws in metallic structures, BS 7910:2013, The British Standards Institution, 2013.
[2] Doyle PA, Scala CM. Crack depth measurement by ultrasonics: a review. Ultrasonics 1978;16:164–70.
[3] Blitz J, Simpson G. Ultrasonic methods of non-destructive testing. 1st ed. London: Champman & Hall; 1996.
[4] Silk MG, Lidington BH. The potential of scattered or diffracted ultrasound in the determination of crack depth. Non-Destr Test 1975;8:146–51.
[5] Silk MG. Defect sizing using ultrasonic diffraction. Br J Non-Destr Test 1979;21:12–5.
[6] Baby S, Balasubramanian T, Pardikar RJ, Palaniappan M, Subbaratnam R. Time-of-flight diffraction (TOFD) technique for accurate sizing of surface-breaking cracks. Insight 2003;45:426–30.
[7] Holmes C, Drinkwater BW, Wilcox PD. Post-processing of the full matrix of ultrasonic transmit-receive array data for non-destructive evaluation. NDTE Int 2005;38:701–11.
[8] Zhang J, Velichko A, Drinkwater BW, Wilcox PD. The characterization of crack-like defects using ultrasonic images. In: Proceedings of the AIP conference; 2010. 1211. pp. 895–902.
[9] Zhang J, Drinkwater BW, Wilcox PD. Defect characterization using an ultrasonic array to measure the scattering coefficient matrix. IEEE Trans Ultrason Ferroelectr Freq Control 2008;55:2254–65.
[10] Zhang J, Drinkwater BW, Wilcox PD, Hunter AJ. Defect detection using ultrasonic arrays: the multi-mode total focusing method. NDTE Int 2010;43:123–33.
[11] Mahaut S, Leymarie N, Poidevin C, Fouquet T, Dupond O. Study of complex ultrasonic NDT cases using hybrid simulation method and experimental validations. Insight 2011;53:664–7.
[12] Schmerr LW. Fundamentals of ultrasonic nondestructive evaluation: a modeling approach. New York: Plenum; 1998.
[13] Velichko A, Wilcox PD. Efficient finite element modeling of elastodynamic scattering with non-reflecting boundary conditions. In: Proceedings of the AIP conference; 2012. 1430. pp. 142–149.
[14] Velichko A, Wilcox PD, Drinkwater BW. Detection of near-surface and surface-breaking defects using ultrasonic arrays. In: Proceedings of the AIP conference; 2012. 1430. pp. 929–936.
[15] Felice MV, Velichko A, Wilcox PD, Barden TJ, Dunhill TK. Simulation of the ultrasonic array response from real branched cracks using an efficient finite element method. In: Proceedings of the AIP conference; 2014. 1581. pp. 100–107.
[16] Wilcox PD, Velichko A. Efficient frequency-domain finite element modeling of two-dimensional elastodynamic scattering. J Acoust Soc Am 2010;127:155–65.
[17] Miller GF, Pursey H. The field and radiation impedance of mechanical radiators on the free surface of a semi-infinite isotropic solid. Proc R Soc Lond A 1954;223:521–41.
[18] Chiao RY, Thomas LJ. Analytical evaluation of sampled aperture ultrasonic imaging techniques for NDE. IEEE Trans Ultrason Ferroelectr Freq Control 1994;41:484–93.